JVSTB Journal of Vacuum Science & Technology B

High performance lithium niobate surface acoustic wave transducers in the 4–12 GHz super high frequency range

Xiao Chen, Mohammad Ali Mohammad, James Conway, Bo Liu, Yi Yang, and Tian-Ling Ren

Citation: Journal of Vacuum Science & Technology B **33**, 06F401 (2015); doi: 10.1116/1.4935561
View online: http://dx.doi.org/10.1116/1.4935561
View Table of Contents: http://scitation.aip.org/content/avs/journal/jvstb/33/6?ver=pdfcov
Published by the AVS: Science & Technology of Materials, Interfaces, and Processing

High performance lithium niobate surface acoustic wave transducers in the 4–12 GHz super high frequency range

Xiao Chen[a] and Mohammad Ali Mohammad[a]
Institute of Microelectronics and Tsinghua National Laboratory for Information Science and Technology (TNList), Tsinghua University, Beijing 100084, China

James Conway
Stanford Nanofabrication Facility (SNF), Stanford University, Stanford, California 94305

Bo Liu, Yi Yang, and Tian-Ling Ren[b]
Institute of Microelectronics and Tsinghua National Laboratory for Information Science and Technology (TNList), Tsinghua University, Beijing 100084, China

(Received 16 July 2015; accepted 30 October 2015; published 16 November 2015)

Surface acoustic wave (SAW) transducers are a well-established component used in numerous sensors, communications, and electronics devices. In this work, the authors report a systematic study of 320–800 nm period lithium niobate SAW interdigitated transducers (IDTs) corresponding to resonant frequencies in the 4–12 GHz range. An optimized SAW design and a nanofabrication process flow were developed, which enabled superior device performance in terms of frequency, signal losses, and electromagnetic coupling. The influence of the device alignment on the substrate crystal planes, in addition to the IDT period and electrode design, is found to have a significant impact on various process metrics. As an example, two identical SAW transducers fabricated perpendicular to each other may have a resonant frequency difference approaching 1 GHz, for the same harmonic mode. These and other trends are presented and discussed. © *2015 American Vacuum Society*. [http://dx.doi.org/10.1116/1.4935561]

I. INTRODUCTION

Surface acoustic wave (SAW) transducers are an essential component of numerous communications and electronics devices. SAW transducers were introduced as filters in cell phones over two decades ago;[1,2] however, they were in use in other telecommunication and microwave applications since the early 1970s.[3] More recently, they have also been used in touch screens,[4] for microfluidics,[5] and in advanced optomechanical research.[6] In addition, a plethora of sensors make use of SAW devices, such as for sensing temperature,[7] acceleration,[8] various gases,[9] biological molecules,[10] etc. SAW transducers convert an electrical signal to an acoustic wave, which travels on the surface of the material used to generate the wave. A typical SAW device consists of one or more sets of comb-like interdigitated transducers (IDTs) fabricated on a piezoelectric substrate [see Fig. 1(a)]. The acoustic wave is generated perpendicular to the direction of the IDTs, where it travels on the surface and interacts with other structures (e.g., gratings, pads, etc.) and reflects back. The interaction of the reflected wave with the incident acoustic wave gives rise to a resonance peak.

The resonance peak has various performance metrics such as frequency (f), amplitude, bandwidth, quality factor (Q-factor), etc. Other information that can be obtained from the resonance peak include electromechanical coupling coefficient (k^2_{eff}) and, in the case of a two-port SAW device, transmission loss. The properties of the acoustic wave, such as the frequency, depends on the piezoelectric substrate material and the IDT period λ, where $\lambda = 4 \times$ IDT linewidth (LW). The IDT LW is also often referred to in literature as the IDT finger width. The speed of sound (ν) in any given material is an intrinsic property of the material and hence it impacts other properties ($f = \nu/\lambda$) accordingly. However, in the case of the IDT period, a smaller λ IDT can be fabricated

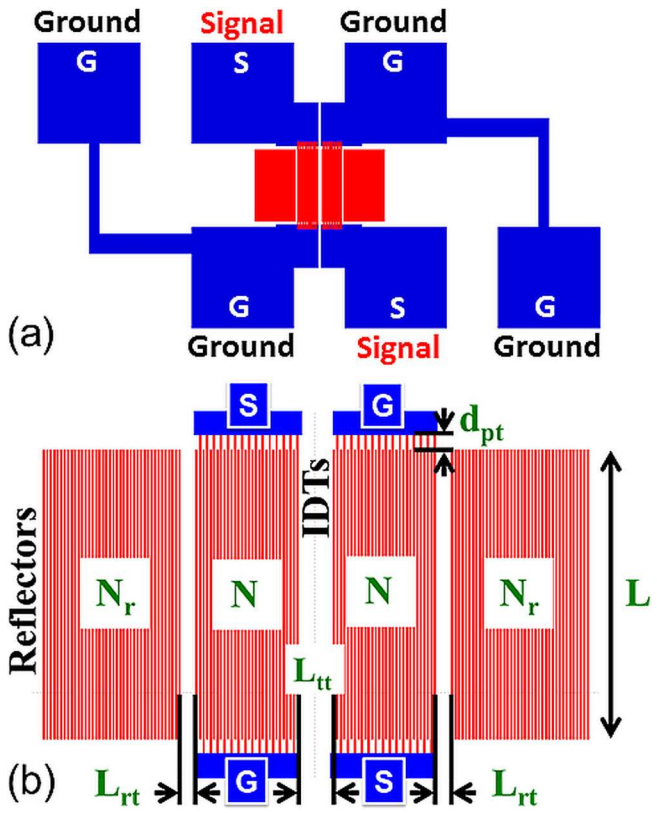

FIG. 1. (Color online) Two-port (a) SAW device design with GSG electrode configuration, and (b) the magnified IDTs and reflectors structure with relevant labels.

[a]X. Chen and M. A. Mohammad contributed equally to this work.
[b]Electronic mail: RenTL@tsinghua.edu.cn

enabling a higher resonant frequency. A higher frequency in turn enables faster data transfer rates,[11] improved selectivity for sensors,[12] and opens a window for advanced research in optoacoustics.[13] Recently, there has been renewed interest in using SAW transducers for short range, high speed communications such as between computer peripherals, such as wireless identity tags,[14] and for the *internet of things* in general.[15]

Lithium niobate ($LiNbO_3$) is an established piezoelectric material used in SAW devices with a moderately high acoustic wave speed (3488–4750 m/s), a high k^2_{eff} (up to 15.8%), low acoustic transmission loss, and a high stability.[2] An in-depth literature review suggests that there have been a number of efforts toward the development of $LiNbO_3$ SAW devices in the super-high frequency (SHF) regime. From 1997 to 1998, three publications[16–18] from the same group (Yamanouchi and Odagawa) reported 5–15 GHz filter devices using 128°YX $LiNbO_3$. Although the complete design and fabrication conditions have not been reported in these works, at least one paper describes that the smallest device period obtained was 380 nm (LW = 95 nm) fabricated using electron beam lithography (EBL). In 2002 and 2003, Takagaki *et al.*[19] and Makkonen *et al.*[20] reported 7.3 GHz ($\lambda = 600$ nm, nanoimprint lithography) and 5.5 GHz ($\lambda = 1200$ nm, optical lithography) devices, respectively. Finally, after nearly a decade, in 2011, Chen *et al.*[21] reported 8.7 GHz ($\lambda = 400$ nm) devices using nanoimprint lithography and YZ $LiNbO_3$ substrate. In terms of performance metrics, whereas the frequency and losses information can be obtained from all of the papers, none report the k^2_{eff}. Nevertheless, if the search is not limited to contemporary high frequency $LiNbO_3$ SAW devices, k^2_{eff} up to 15.8%,[2] 11%,[22] 9.6%,[19] and 8.4% (Ref. 23) can be obtained, which ranges from a few times higher to up to 2 orders of magnitude higher when compared to other piezoelectric materials.

Given the importance of high frequency SAW devices described earlier and the current state of the literature, there is much to understand about the design, fabrication, and operation of $LiNbO_3$ SAW devices in the SHF regime (generally defined as 3–30 GHz). In this work, we systematically study the low to middle range of the SHF regime by fabricating $LiNbO_3$ SAW devices operating from approx. 4–12 GHz. We carefully consider the effects of the electrode and IDT design, IDT period, and IDT orientation on the substrate. The fabrication process is carefully controlled, and a wide range of performance metrics and trends are obtained and discussed.

TABLE I. SAW IDT partial design parameters.[a]

λ (nm)	LW (nm)	L (μm)	L_{tt} (μm)	L_{rt} (μm)	Dose (μC/cm^2)	Factor
320	50	23 (~72 λ)	2.24 (n = 7)	1.04 (n = 7)	158	1.44
400	80	29 (~72 λ)	2.0 (n = 5)	0.9 (n = 5)	151	1.37
600	150	43 (~72 λ)	3.0 (n = 5)	1.35 (n = 5)	156	1.42
800	200	52 (~65 λ)	4.0 (n = 5)	1.8 (n = 5)	147	1.34

[a]The symbols are explained in Sec. II A and depicted in Fig. 1(b).

II. EXPERIMENT

A. SAW transducer design

The structure of the SAW devices used in this work is shown in Fig. 1(a). This is a two-port type device, which is symmetric from both IDT design and electrical signal input/output perspective. There are two sets of IDTs and reflectors in the center of the SAW device, which is shown in more detail in Fig. 1(b). The various quantities and dimensions used in the design, labeled on Fig. 1(b), are determined by various empirical formulae and knowledge.[24] The number of IDT pairs N is kept constant at 25, and the number of reflector pairs $N_r = 2 \times N$ and is therefore kept constant at 50. The IDT period (λ) is given by $\lambda = 2 \times (a + b)$, where a and b are the IDT finger width or LW and the IDT spacing, respectively. Both λ and LW are variables whose values are shown in Table I. For the 320 and 400 nm smaller period devices, LW $< \lambda/4$, which is a deliberate design bias so that the metallization ratio a/b approaches unity once the fabrication is complete. The length of the IDTs is given by $L = k \times \lambda$, where k is a positive integer with a constraint $50 \leq k \leq 100$. The spacing between the IDTs and reflectors is given by the formula $L_{rt} = [n - (1/2)]\lambda/2$, where n is a positive odd integer, e.g., 5, 7, etc. Similarly, the spacing between both IDTs is given by $L_{tt} = m(\lambda/2)$, where $m = 2 \times n$. The design parameter values for L, L_{rt}, L_{tt}, k, and n are also listed in Table I, along with the exposure dose and dose factor (explained ahead) for each SAW IDT period.

The SAW devices are designed such that the distance between the signal electrodes and the IDTs is kept to a minimum. Furthermore, the electrodes are designed in a way that the electrical signal is given a low-resistance path by using a large connecting interface and avoiding any "neck-like" narrow trace paths. The design is better understood by comparing the present version [Figs. 1(a) and 1(b)] with an older design [supplementary Fig. S1 (Ref. 25)]. The distance between the electrodes and IDTs d_{pt} [Fig. 1(b)] is kept constant at 2 μm. Each SAW device is fabricated in pairs, one perpendicular to the other. Since the $LiNbO_3$ used in this work is not a single crystal substrate as shown by x-ray diffraction (XRD) results (supplementary Fig. S2),[25] the acoustic wave properties such as the velocity, losses, etc., will differ according to crystal plane. Consequently, the orientation of the devices on the substrate is of key importance. The perpendicularly oriented devices are differentiated by the labels horizontal (H-) and vertical (V-) type in this paper. Except for the 90° rotation, both H-type and V-type SAW devices are identical.

B. SAW transducer fabrication and characterization

A set of 128°YX $LiNbO_3$ substrates were diced into 1×1.5 cm^2 chips, subjected to piranha cleaning (H_2SO_4:H_2O_2 3:1) for 15 min, rinsed in deionized (DI) H_2O, and baked at 175 °C for 5 min. The prepared substrates were spun cast with PMMA 950k EL4 resist (Allresist GmbH) at 4000 rpm yielding an approx. 200 nm thick layer. The PMMA coated substrates were prebaked at 175 °C for 5 min and allowed to cool

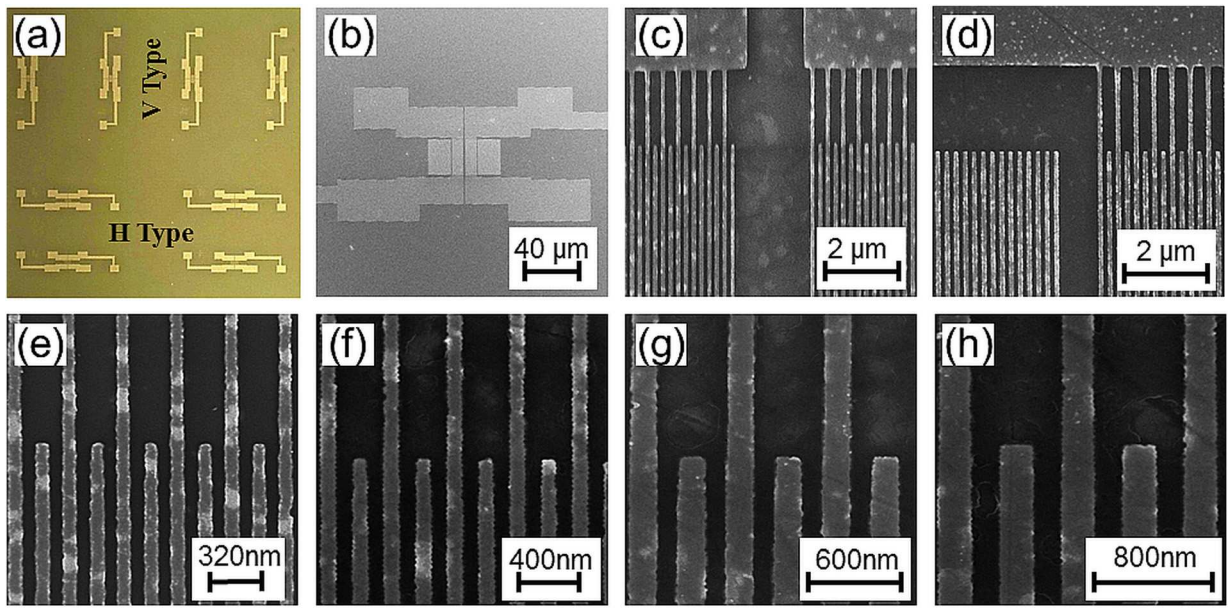

FIG. 2. (Color online) Optical microscope images of (a) fabricated H-type and V-type SAW devices. SEM micrographs of 400 nm period SAW devices showing (b) central region, (c) magnified region between two IDTs, and (d) magnified region between an IDT and a reflector. High resolution SEM micrographs of (e) 320 nm, (f) 400 nm, (g) 600 nm, and (h) 800 nm period IDTs. The SEM voltage and working distance are 10 keV and 5 mm, respectively. The bright patterns in panels (c)–(f) are possibly charging artefacts caused due to defects (notching) in the thin EPACER layer spun-cast before SEM imaging.

down ($\geq$1 h). As the $LiNbO_3$ substrates are nonconductive and prone to severe charging under an electron beam, a thin conductive layer of ESPACER ($\sim$20 nm at 2000 rpm)[26] was spun on top of the PMMA. The SAW transducer patterns were exposed at 10 keV using a Raith 150^{TWO} EBL tool. On each chip, both H- and V-type patterns were exposed, and the IDT periods and applicable doses used are as described in Table I. Following the EBL exposure, a 30 s immersion in DI H_2O was used to remove the ESPACER film. Development was subsequently carried out in methyl isobutyl ketone: isopropyl alcohol 1:3 at room temperature for 10 s. Electron beam evaporation (Kurt J. Lesker) was used for metallization, which consisted of a Ti seed layer (8–10 nm) followed by an Au layer (26–30 nm). The total thickness of the Au/Ti stack was kept between 34 and 40 nm, with smaller IDT periods subjected to slightly thinner metal layers for easier liftoff. Finally, the liftoff was performed in acetone (1–5 min) using an ultrasonic bath and the chips were dried with N_2. The end of the liftoff process was inspected visually with the naked eye and also using an optical microscope prior to N_2 drying.

The EBL exposure doses are determined separately for each SAW IDT period [see supplementary Fig. S3 (Ref. 25)]. A specially designed dose-test optimization pattern, with inspiration from Ref. 27, is fabricated using the steps defined above and characterized using scanning electron microscopy (SEM). This process is repeated for each IDT period. SEM inspection is used to identify the area dose factor for which the electrode and IDTs are fabricated simultaneously with good quality [see supplementary Fig. S3 (Ref. 25)]. The identified area dose factor is then used (area dose = area dose factor $\times$ base dose) for fabrication of the actual SAW devices. In this work, a base dose of 110 μC/cm^2 is used, and the area doses and dose factors are listed in Table I. The electrodes use a unity dose factor.

The fabricated SAW devices are inspected with scanning electron microscopy using an FEI Nova 650 SEM and a Raith 150 (Zeiss Gemini^{TM} column) for IDT dimension measurements and overall quality. Prior to inspection, the completed chips are coated with ESPACER again to prevent charging and to prevent contamination marks from being deposited on the surface during microscopy. The ESPACER is washed-off using DI water after inspection, as described previously.

Figure 2 presents fabrication results of selected SAW devices. An optical microscope image of a patterned $LiNbO_3$ chip [Fig. 2(a)] shows various H- and V-type devices. A SEM micrograph of the central region of a 400 nm period SAW device [Fig. 2(b)] shows the relative position of the electrodes, IDTs, and fabrication quality. Magnifying further into this device, the central region between two IDTs [Fig. 2(c)], and the region between an IDT and a reflector [Fig. 2(d)] can be observed. Both panels (c) and (d) demonstrate the horizontal (inner versus outer IDTs) and vertical (upper versus lower) uniformity of the IDTs as well as the clean interface between the electrodes and the IDTs. Achieving such uniformity is not straightforward. Since SAW devices have a complex geometry and are fabricated using EBL on nonconductive substrates, charging and proximity effects play a significant role.

The linewidths (previously labeled a or LW) are quite uniform as the exposure doses have been determined by a dose optimization strategy using a specially designed "dose-test" pattern [supplementary Fig. S3 (Ref. 25)]. Without using such a process for determining the doses, the lines become very narrow in the 2 μm region between the electrodes and overlapping dense IDTs region. The lines may even break [supplementary Fig. S3(e)][25] or vanish altogether. Despite this process, some nonuniformity can be observed

due to the proximity effect, e.g., the 400 nm period IDTs [Figs. 2(c) and 2(d)] have a LW = 92 nm in the 2 μm upper region and a LW = 98 nm in the lower dense IDT region. SEM images of the 320–800 nm period IDTs are shown in Figs. 2(e)–2(h). The corresponding LW measured from the dense IDT regions are 81, 98, 168, and 212 nm, respectively. These measurements are approx. 1/4th of the IDT period or correspond to a 50% metallization ratio ($a/b \sim 1$).

C. SAW transducer frequency testing

The frequency characteristics of the SAW transducers are measured using an Agilent N5230C network analyzer equipped with a ground-signal-ground (GSG) probe station. The structure of the GSG probes is shown in supplementary Fig. S4.[25] The intermediate frequency is set to 1 kHz, step size is 1 MHz, and AC sweep range varies according to device period within the range of 1–15 GHz. Crystallographic orientation data of the $LiNbO_3$ substrate (supplementary Fig. S2)[25] are obtained using a Rigaku D/Max 2550HB+/PC XRD system with Cu Kα irradiation ($\lambda = 1.54$ Å).

III. TESTING RESULTS AND DISCUSSION

The reflectance (S_{11}) and transmittance (S_{21}) S-parameters obtained via resonance testing are shown in Fig. 3. This includes data of 320–800 nm periods for both H- and V-type devices. Since the two-port devices used in this work are symmetric, we observe $S_{11} = S_{22}$ and $S_{12} = S_{21}$. From Fig. 3, we can obtain or identify certain performance metrics directly, such as the frequency, amplitude, insertion loss (IL), and mode type/number. Other performance metrics, such as the Q-factor, bandwidth, and electromagnetic coupling coefficient (k^2_{eff}) require some straightforward calculations using information obtained from the S-parameter plots. The formula for calculating k^2_{eff} is given by $k^2_{\text{eff}} = (\pi^2/4) \times (f_p - f_s/f_p)$, where f_p and f_s refer to parallel and series frequencies, respectively. Also, strictly speaking, IL can only be used for a SAW filter device; however, in this case, it is somewhat loosely used to refer to the losses in the transmittance (S_{21}) S-parameters of a two-port device.

Inspecting Fig. 3, it can be observed for both H- and V-type devices that the resonance peaks lie between approx. 4–12 GHz with smaller IDT periods exhibiting higher frequencies. Scaling down the IDT period visibly increases the frequency; however, the insertion loss increases, and the signal amplitude degrades to some extent. Comparing H- and V-type devices, it can be observed that H-type devices show three modes (fundamental + two higher harmonics), whereas the V-type devices show one or two modes (fundamental + one higher harmonic). Furthermore, the V-type devices exhibit a higher frequency as compared to H-type devices when considering the same mode. Although the cause of the V-type devices exhibiting higher frequencies is not understood; however, this is plausible as different crystal orientations have different physical properties. A device aligned parallel or perpendicular to a given crystal plane will then also exhibit different properties.

Figure 4 compares the 320 and 400 nm periods for H- and V-type devices separately. It is obvious that the V-type

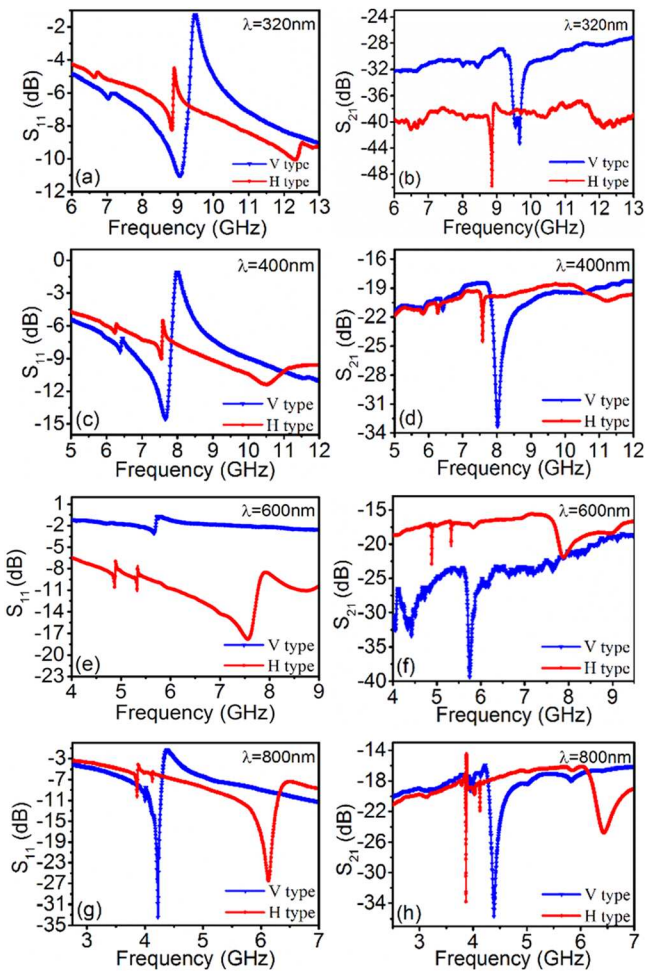

FIG. 3. (Color online) Reflection (S_{11}) and transmission (S_{21}) parameters, respectively, for [(a) and (b)] 320 nm, [(c) and (d)] 400 nm, [(e) and (f)] 600 nm, and [(g) and (h)] 800 nm period SAW devices. Each panel contains spectra for both H-type (triangles) and V-type (circles) devices.

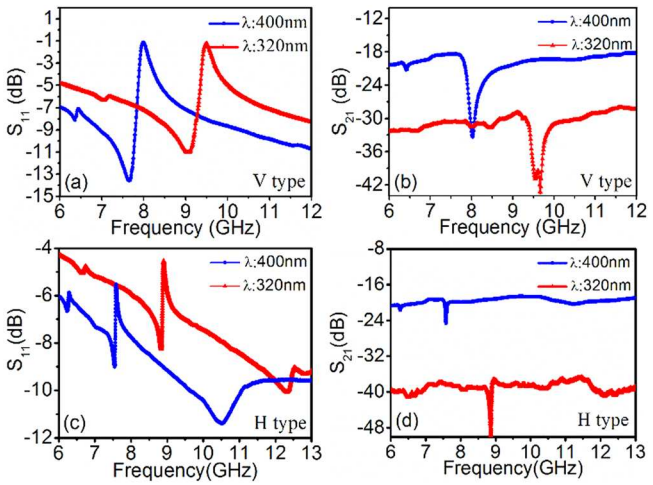

FIG. 4. (Color online) Comparing frequency characteristics of 320 vs 400 nm SAW devices. Reflection (S_{11}) and transmission (S_{21}) parameters, respectively, for [(a) and (b)] V-type, and [(c) and (d)] H-type devices. Each panel contains spectra for both 320 nm (triangles) and 400 nm (circles) period devices.

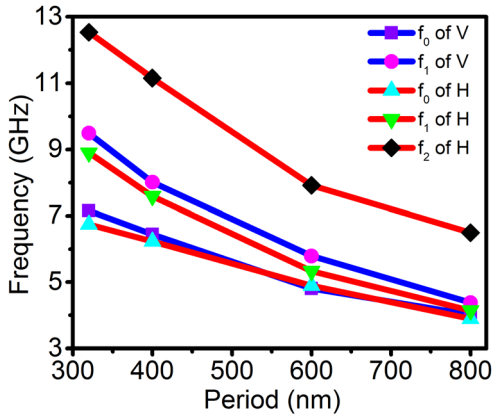

FIG. 5. (Color online) Resonant frequency vs IDT period for both H-type and V-type devices. Trends are shown for various resonant modes.

devices exhibit a higher frequency. Comparing panel of Figs. 4(b) and 4(d), it can be seen that the first order harmonic of the 400 nm period devices differ by nearly 400 MHz (V-type 8 GHz versus H-type 7.6 GHz). Similarly, the 320 nm period devices differ by nearly 800 MHz (V-type 9.7 GHz versus H-type 8.9 GHz). The frequencies reported herein are extraordinary as well. The 9.7 GHz V-type peak exceeds the recently reported results[21] exploring a regime of operation hardly elucidated for $LiNbO_3$. The IL also compares favorably at 29.2 dB (this work) vs 61.7 dB.[21] Furthermore, the H-type second order mode 12.2 GHz peak [Figs. 4(c) and 4(d)] is at an even higher frequency, albeit with lower amplitude and greater losses, hence reducing the utility.

The frequency versus period is plotted in Fig. 5 showing detailed trends for both H- and V-type devices and all operational modes. Given the relation $f = \nu/\lambda$, where ν is the sound velocity, the trends are according to expectation. For the H-type devices (first order mode), ν increases from 2848 to 3280 m/s as one increases the period from 320 to 800 nm. Similarly, for the V-type devices (first order mode), ν increases from 3104 to 3520 m/s. These values are acceptable

TABLE II. Performance metrics of H-Type SAW devices for the zeroth, first, and second harmonic.

λ (nm)	f_0 (GHz)	Q_p	IL (dB)	k^2_{eff} (%)
320	6.7	—	—	3.5
400	6.2	—	20.7	2.0
600	4.9	444	17.0	0.9
800	3.9	1933	18.9	0.6
f_1 (GHz)				
320	8.9	443	38.5	1.8
400	7.6	180	19.9	1.2
600	5.3	266	17.0	0.5
800	4.1	688	18.0	0.4
f_2 (GHz)				
320	12.5	—	—	4.1
400	11.2	—	—	—
600	7.9	14	15.6	11.0
800	6.5	21	19.0	13.6

TABLE III. Performance metrics of V-type SAW devices for the first harmonic.

λ (nm)	f_1 (GHz)	Q_p	IL (dB)	k^2_{eff} (%)
320	9.5	190	29.2	11.0
400	8.0	81	19.3	10.7
600	5.8	125	23.7	5.3
800	4.4	116	17.4	8.8

as previously reported sound velocities in $LiNbO_3$ range from 3488 to 4750 m/s.[2] Furthermore, the gradual reduction of ν with λ is expected as smaller periods have narrower IDT linewidths, which in turn have increased resistance to signal flow.

The SAW device performance metrics for H- and V-type devices are summarized in Tables II and III, respectively. In addition to the aforementioned trends, it can also be seen that the Q-factor for the H-type SAW devices is better than the V-type devices. Here, the Q-factor is calculated using the parallel frequency, hence the symbol Q_p is used in Tables II and III. On the other hand, the k^2_{eff} for the V-type devices is better than the H-type devices. Both V- and H-type (f_0, f_1) devices exhibit a gradually increasing trend of k^2_{eff} with decreasing period. This implies that scaling the devices down improves the electrical to mechanical conversion efficiency and the bandwidth. A survey of recent literature shows that our observation is supported by Refs. 28 and 29, partially supported (i.e., for some modes) by Ref. 30, and opposed by Ref. 31; however, none of these works highlight or discuss this intriguing aspect. The relationship of k^2_{eff} with IDT period requires an in-depth investigation. In summary, when comparing the H- and V-type devices, it can be seen that the V-type devices have a higher frequency and k^2_{eff} as compared to the H-type devices. The H-type devices have a higher Q-factor and display more modes.

Finally, when comparing this work to previous high frequency $LiNbO_3$ SAW research works, our efforts are superior in terms of the period, linewidth, and k^2_{eff} achieved. The comparison can be understood in detail via supplementary Table T1 (Ref. 25) and the literature review in Sec. I. The frequency and losses are also excellent and exceed all previous $LiNbO_3$ results with the exception of the pioneering works conducted by Yamanouchi and Odagawa.[16–18] In terms of metrics, our results are comparable to these exceptional pioneering works; however, we systematically investigate various aspects of high frequency $LiNbO_3$ SAW devices in much greater depth. The foundation laid in this work can be used to further advance the investigation of super high frequency $LiNbO_3$ SAW devices.

IV. SUMMARY AND CONCLUSIONS

SAW transducers with 320–800 nm IDT periods were fabricated and tested. An optimized design and nanofabrication process flow enables generally superior fabrication and process metrics, as compared to other contemporary research works with $LiNbO_3$, including period and linewidth, frequency, k^2_{eff}, and IL. A systematic study of SAW transducers considering the electrode design, IDT periods, crystal alignments, and

resonance modes enables an in-depth insight into the various trends. It is observed that scaling down the device dimensions increases the frequency and k^2_{eff} at the cost of IL and resonant signal amplitude. For any given mode (harmonic), V-type devices yield a higher frequency and k^2_{eff}; however, H-type devices yield a higher Q-factor. The H-type devices also exhibit a greater number of modes. The highest frequencies reported in this work are 9.7 GHz (V-type, first order mode) and 12.2 GHz (H-type, second order mode). Further work is being carried out to (1) increase the resonant frequency, (2) reduce the losses through improved nanofabrication, and (3) theoretically investigate the dependence of performance on SAW device alignment to various crystal orientations. The results presented in this work can be used as a foundation for highly sensitive sensors and other applications development.

ACKNOWLEDGMENTS

The authors acknowledge the facilities and staff members at the following four institutes where this work was conducted: (1) Institute of Microelectronics at Tsinghua University, (2) Key Laboratory for the Physics and Chemistry of Nanodevices, Department of Electronics, Peking University, (3) Institute of Microelectronics of the Chinese Academy of Sciences, and (4) Institute of Semiconductors of the Chinese Academy of Sciences. Funding is gratefully acknowledged from the National Natural Science Foundation (61434001), the 973 Program (2015CB352100), the National Key Project of Science and Technology (2011ZX02403-002), and the Special Fund for Agroscientific Research in the Public Interest (201303107) of China. M.A.M. gratefully acknowledges postdoctoral fellowship (PDF) funding from the Natural Sciences and Engineering Research Council (NSERC) of Canada and from the China Postdoctoral Science Foundation (2014M560080).

[1]C. K. Campbell, *Surface Acoustic Wave Devices for Mobile and Wireless Communications* (Academic, San Diego, CA, 1998).
[2]C. C. W. Ruppel, L. Reindl, and R. Weigel, IEEE Microwave Mag. **3**, 65 (2002).
[3]R. M. Hays and C. S. Hartmann, Proc. IEEE **64**, 652 (1976).
[4]T. Katsuki, F. Nakazawa, S. Sano, Y. Takahashi, and Y. Satoh, "A compact and high optical transmission SAW touch screen with ZnO thin-film piezoelectric transducers," *IEEE Symposium on Ultrasonics* (2003), pp. 821–824.
[5]X. Ding *et al.*, Lab Chip **13**, 3626 (2013).
[6]D. A. Fuhrmann, S. M. Thon, H. Kim, D. Bouwmeester, P. M. Petroff, A. Wixforth, and H. J. Krenner, Nat. Photon. **5**, 605 (2011).
[7]A. Kang, C. Zhang, X. Ji, T. Han, R. Li, and X. Li, Sens. Actuators A **201**, 105 (2013).
[8]W. Wang, Y. Huang, X. Liu, and Y. Liang, Smart Mater. Struct. **24**, 015015 (2015).
[9]W. P. Jakubik, Thin Solid Films **520**, 986 (2011).
[10]K. Länge, B. E. Rapp, and M. Rapp, Anal. Bioanal. Chem. **391**, 1509 (2008).
[11]C. C. W. Ruppel, N. Geng, A. Waldherr, and R. Dill, "Surface acoustic wave devices for wireless local area networks," http://www.te.chiba-u.jp/~ken/Symp/Symp2001/PAPER/CLEMENS.PDF, Last accessed October 17, 2015 (2001).
[12]H.-L. Cai *et al.*, Biosens. Bioelectron. **71**, 261 (2015).
[13]S. A. Tadesse and M. Li, Nat. Commun. **5**, 5402 (2014).
[14]V. P. Plessky and L. M. Reindl, IEEE Trans. Ultrason. Ferroelectr. **57**, 654 (2010).
[15]D. W. Lv, X. J. Li, L. X. Yang, D. J. Liu, K. Xiong, X. B. Liang, S. F. Li, and B. Zhang, Appl. Mech. Mater. **738–739**, 125 (2015).
[16]K. Yamanouchi, J. A. Qureshi, and H. Odagawa, "5-15 GHz range surface acoustic wave filters using electrode thickness difference type and new reflector bank type of unidirectional interdigital transducers," *Proceedings of the Ultrasonics Symposium* (1997), pp. 61–64.
[17]H. Odagawa and K. Yamanouchi, "10 GHz range extremely low-loss ladder type surface acoustic wave filter," *Proceedings of the Ultrasonics Symposium* (1998), pp. 103–106.
[18]K. Yamanouchi, "Generation, propagation, and attenuation of 10GHz-range SAW in $LiNbO_3$," *Proceedings of the Ultrasonics Symposium* (1998), pp. 57–62.
[19]Y. Takagaki, E. Wiebicke, H. Kostial, and K. H. Ploog, Nanotechnology **13**, 15 (2002).
[20]T. Makkonen, V. P. Plessky, W. Steichen, S. Chamaly, C. Poirel, M. Solal, and M. M. Salomaa, Appl. Phys. Lett. **83**, 3596 (2003).
[21]N.-H. Chen, J.-C. Huang, C.-Y. Wang, and F.-S. Huang, J. Micromech. Microeng. **21**, 045021 (2011).
[22]K. Yamanouchi and K. Shibayama, J. Appl. Phys. **43**, 856 (1972).
[23]D. Ciplys and R. Rimeika, Ultragarsas **3**, 14 (1999) available at http://www.ultragarsas.ktu.lt/index.php/USnd/article/view/7945/3938.
[24]Z. ChangJian, "Research on the key issues of high-frequency acoustic resonator based on piezoelectric films," Ph.D. thesis (Tsinghua University, 2012).
[25]See supplementary material at http://dx.doi.org/10.1116/1.4935561 for additional design, fabrication, and testing information. This file also contains a comparison with previous high frequency $LiNbO_3$ SAW devices.
[26]K. K. Showa Denko, "ESPACER technical report," http://www.showa-denko.com/wp-content/uploads/2014/05/ESP_Technical_Report.pdf, Last accessed October 17, 2015.
[27]M. A. Mohammad, "Investigation of electron beam nanolithography processes, mechanisms, and applications," Ph.D. thesis (University of Alberta, 2013).
[28]C. Zhou, Y. Yang, H. Jin, B. Feng, S. Dong, J. Luo, T.-L. Ren, M. Chan, and C. Y. Yang, Thin Solid Films **548**, 425 (2013).
[29]C. Zhou, Y. Yang, H. Cai, T.-L. Ren, M. Chan, and C. Y. Yang, IEEE Electron Device Lett. **34**, 1572 (2013).
[30]S. Büyükköse, B. Vratzov, D. Ataç, J. van der Veen, P. V. Santos, and W. G. van der Wiel, Nanotechnology **23**, 315303 (2012).
[31]A. B. A. Dow, C. Popov, U. Schmid, and N. P. Kherani, IEEE Trans. Ultrason. Ferroelectr. **60**, 1581 (2013).